



Particle detection, number estimation, and feature measurement in gene transfer studies: optical fractionator stereology integrated with digital image processing and analysis

Michael A. King,^{a,b,c,*} Nicole Scotty,^{b,d} Ronald L. Klein,^{b,d} and Edwin M. Meyer^{b,d}

^a Veterans Administration Medical Center, Research Services 151, University of Florida, Gainesville, FL 32602, USA

^b University of Florida Brain Institute, University of Florida College of Medicine, Gainesville, FL 32610, USA

^c Department of Neuroscience, University of Florida College of Medicine, Gainesville, FL 32610, USA

^d Department of Pharmacology and Therapeutics, University of Florida College of Medicine, Gainesville, FL 32610, USA

Accepted 15 July 2002

Abstract

Assessing the efficacy of in vivo gene transfer often requires a quantitative determination of the number, size, shape, or histological visualization characteristics of biological objects. The optical fractionator has become a choice stereological method for estimating the number of objects, such as neurons, in a structure, such as a brain subregion. Digital image processing and analytic methods can increase detection sensitivity and quantify structural and/or spectral features located in histological specimens. We describe a hardware and software system that we have developed for conducting the optical fractionator process. A microscope equipped with a video camera and motorized stage and focus controls is interfaced with a desktop computer. The computer contains a combination live video/computer graphics adapter with a video frame grabber and controls the stage, focus, and video via a commercial imaging software package. Specialized macro programs have been constructed with this software to execute command sequences requisite to the optical fractionator method: defining regions of interest, positioning specimens in a systematic uniform random manner, and stepping through known volumes of tissue for interactive object identification (optical dissectors). The system affords the flexibility to work with count regions that exceed the microscope image field size at low magnifications and to adjust the parameters of the fractionator sampling to best match the demands of particular specimens and object types. Digital image processing can be used to facilitate object detection and identification, and objects that meet criteria for counting can be analyzed for a variety of morphometric and optical properties.

© 2002 Published by Elsevier Science (USA).

Keywords: Stereology; Morphometry; Histology; Histometry; Object counting

1. Introduction

Gene transfer studies frequently require quantitative assessment of the number of cells that either express the introduced gene(s) [1–3] or respond in some way to transgene expression [4–6]. The development of advanced techniques for quantitative microscopic analysis of structural features in biological materials has stimulated histometrists to adopt unbiased methods for determining the number of objects of interest in tissue specimens [7–11]. Techniques based on the optical dis-

sector, for example, are efficient, relatively simple, and powerful (e.g., [12,13]). In this approach, the plane of focus is passed vertically a known distance through the specimen, and objects are counted according to certain rules. The combination of the optical disector with statistically optimized spatial sampling protocols constitutes the optical fractionator, described as the most efficient unbiased object counting method available [14,15]. Several articles that describe the process of conducting fractionator stereology in detail are available [12,16]. These methods yield unbiased estimates of the total number of objects in a sample with the most efficient investment of counting effort.

One characteristic of the advanced stereological methods is that they depend on precise specimen posi-

* Corresponding author. Fax: 1-352-392-8347.

E-mail address: making@nersp.nerdc.ufl.edu (M.A. King).

tioning for (1) systematic uniform random spatial sampling, (2) moving the plane of focus through a known vertical distance, and (3) precise measurement of section thickness. Because microscopes have historically not been equipped for such tasks, adopting stereological methods frequently necessitates investment in new equipment to monitor and/or control the position of microscopy specimens. This equipment can be as simple as a microcator capable of measuring section thickness with 0.5- μm accuracy; such devices provide satisfactory solutions [17]. However, microcators have few other applications in histomorphometry and provide only measurement in the vertical (Z) dimension and not positional control (focus). Nor do they measure or control stage X and Y positioning, which must be accomplished by other means such as manual relocation and position measurement using stage vernier scales. These can be limited in accuracy, precision, and reproducibility, especially at high magnifications.

Another requirement for stereology is a way to superimpose test grids or counting frames over specimen images. Although eyepiece reticles, image projection tubes, or transparencies can accomplish this, many users find these difficult to use, especially for long periods or with certain specimen preparations.

We have constructed a system of hardware and software for the purpose of conducting stereological studies of sectioned brain. This system permits precise and accurate positioning of samples in three dimensions and carries out the optical fractionator procedures with a minimum of human participation. All of the components are “off the shelf,” except for application macro programs specifically developed to use the optical fractionator. We have used this system to assess the effects of *in vivo* gene transfer on the number of brain neurons expressing defining gene products, either natural or derived from gene transfer vectors.

2. Hardware

The design of the system is presented in Fig. 1. It consists of a conventional optical microscope (Olympus BH-2) equipped with a motorized stage and focus control system (Prior Scientific). These permit positioning accuracy to 1 μm in the XY and 0.1 μm in the Z (depth) dimensions. The microscope is configured with nose-piece objectives ranging from 1 to 100 \times and a 1, 1.25, and 1.5 \times magnification changer. A color NTSC digital video camera (Hitachi KDP-581) attached to the microscope trinocular tube delivers images to a Flashpoint 128 PCI-bus video frame grabber (Integral Technologies) installed in a Pentium (Intel)-based microcomputer running the Windows95 (or higher) operating system (Microsoft). The Flashpoint handles the primary computer graphics functions in addition to live video display

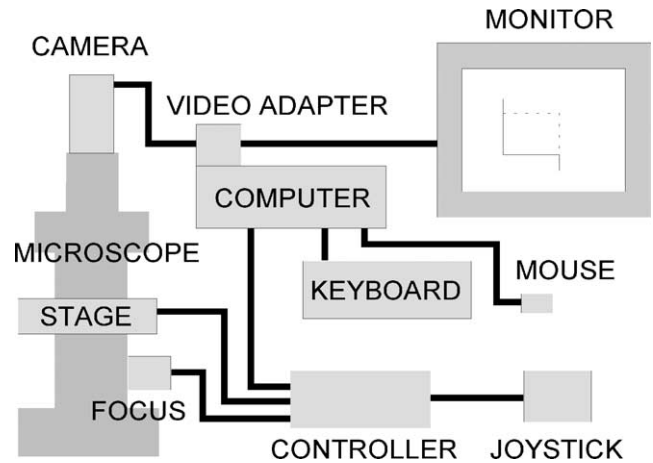


Fig. 1. The hardware involved in the optical fractionator counting/imaging system.

and digitization of video frames. Hardware control of the stage and focus drive motors is mediated by connection of a joystick and focus knob attached to a control box, which is in turn connected to the computer via a serial port.

3. Software

The primary software is ImagePro Plus (Media Cybernetics) version 4.0 or higher, along with the add-on StagePro module for controlling the motorized stage

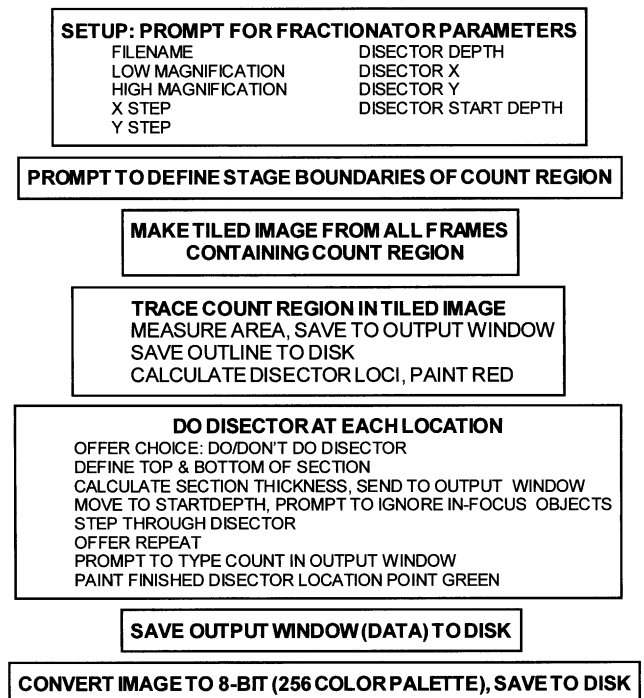


Fig. 2. The flow of the fractionator counting process.

and focus. This software controls the video frame grabber, displaying live video, on demand, in a window on the single monitor. ImagePro Plus also contains a macro development system, based on the BASIC programming language, which permits sequences of commands to be programmed into specialized application modules.

The logical flow of the our Manual Optical Fractionator modules is presented in Fig. 2. The user is first prompted for a file identifier tag, magnifications, and information about the position and size of the individual optical dissectors. Next the user is asked to define, at low magnification ($1\text{--}4\times$ objective), the range of microscope image fields over which the objects of interest are distributed. These boundaries, which can extend to the entire physical XY range of the stage, are used to generate a tiled image (montage, Fig. 3A) containing the entire structure of interest (e.g., tissue section, organ subregion). The upper left corner of this range is set as the zero point from which calibrated stage movements will subsequently refer. The operator then uses the mouse to outline the area in the tiled image in which the dissectors should be generated. The calibrated area of this outline and the outline itself are saved to disk, and the positions of individual dissectors are calculated using the selected magnification and spacing parameters

and the calibrated stage coordinates (Figs. 3A and B). The upper left corner pixel of a rectangle enclosing the traced count region is used as a start point which is for all practical purposes random with respect to the true position of the count region. Each counting location is initially painted as a red box on the low-magnification tiled image. The stage is moved to each of these locations in turn. At each location, the operator is given the option of performing the dissector or not, in case there is some form of artifact preventing object identification. The option to bypass dissector locations should thus be used sparingly.

Because ImagePro Plus does not support overlays onto video, we use an accessory utility provided with the Flashpoint imaging board to view a live video image over which an unbiased, spatially calibrated counting frame appears. To execute the dissector, the operator is prompted to locate the top and bottom surfaces of the tissue section using the focus control knob; the StagePro software tracks the calibrated position of the objective. Section thickness is written to the output window. The objective is moved automatically to the preselected distance above the bottom of the section, where it stops to remind the operator to observe any objects that are in focus at this level (Fig. 3C). These are NOT counted. The focus is then stepped at $1\ \mu\text{m/s}$ through the depth of

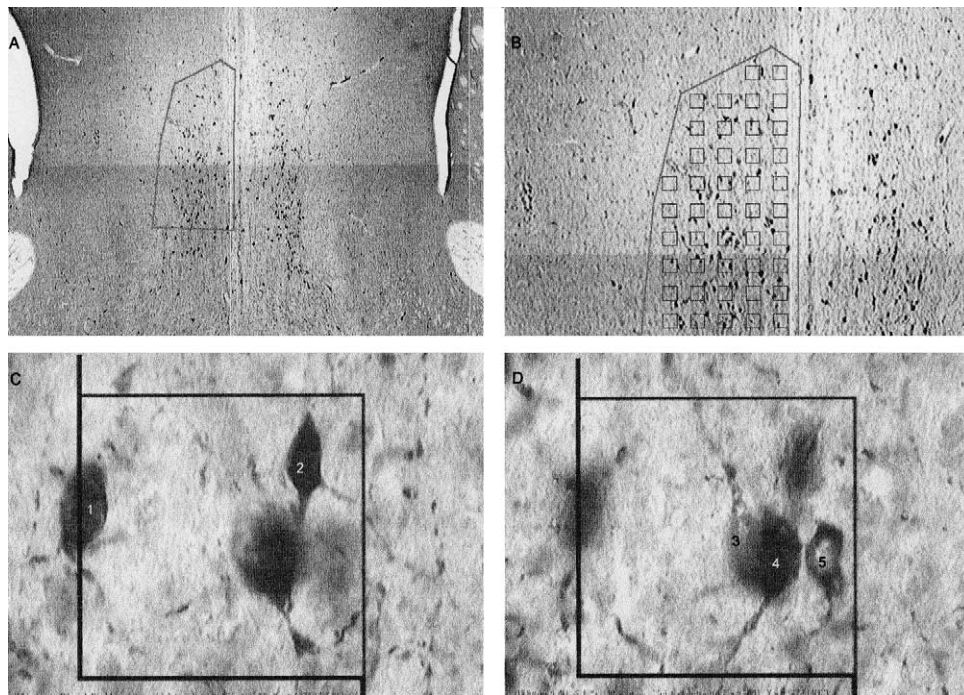


Fig. 3. (A) After making a low-magnification ($4\times$) tiled image of all microscope fields containing the area in which counts are to be made, the count area is identified by outlining on the calibrated image. In this example, the medial septal nucleus is outlined for counting neurons immunolabeled against choline acetyltransferase. (B) Systematic random sampling is used to conduct exhaustive counts in a small fraction of total volume using three-dimensional dissectors of consistent size and spacing. (C) At the bottom focus plane of the dissector, neurons in focus (1, 2) are not included in dissector counts (magnification: $40\times$ nosepiece, $1.25\times$ internal mag. changer, $2.5\times$ camera tube objective). (D) Objects that come into focus above the bottom of the dissector are counted provided that they do not touch the exclusion lines (left and bottom of frame) and lie within or touch the inclusion lines (top and right of frame). Objects 3, 4, and 5 meet these criteria.

the optical dissector. Objects that come into focus anywhere above the bottom level are counted, unless they touch the exclusion lines of the count frame (Fig. 3D). The operator is given the option to repeat the dissector as necessary to ascertain the correct count. When confident of the number of objects, the operator records the count in the output window. Completed dissectors are then painted green on the tiled image, and the stage is moved to the next dissector position. After all dissectors have been completed, an archival image with the count area outline and dissector positions is saved to disk, as is the output window containing all the fractionator parameters used and the thickness and number of objects for each dissector. Because of the regular structure of the output window text file, it is easily imported into common data processing applications software.

The programs provide efficient and precise location and execution of optical dissectors. The output of the program contributes three of the four fractionator quantities necessary to calculate the total object number in a structure: area sampling frequency (ASF; $1/XY$ area between dissectors), thickness sampling frequency (TSF; dissector depth/section thickness), and total number of objects counted in all dissectors ($\sum(n)$). The remaining value, section sampling frequency (SSF), is simply the number of regularly spaced sections used for counts divided by the total number of sections through the structure of interest. These values are used offline to estimate total number of objects (N) in the count region according to Eq. (1) [15]:

$$N = \sum(n) \times 1/SSF \times 1/ASF \times 1/TSF. \quad (1)$$

Estimates of total number, error coefficients (c.e.), average section thickness, average number of objects per dissector, XY , Z , and XYZ sampling fractions, and histograms of number of dissectors containing distinct numbers of objects are calculated from the raw data files using spreadsheet templates. Error coefficients are calculated according to Eq. (2), tested in modeling studies by Glaser and Wilson [20]:

$$\text{c.e.} = 1 / \sqrt{\sum(n)}. \quad (2)$$

Data from a recent gene transfer project illustrate some interesting practical aspects of fractionator counting. An adeno-associated virus vector was used to deliver a mutant α -synuclein (α -syn) gene into the substantia nigra (SN), in an effort to generate a rodent model for a genetic form of Parkinson's disease [6]. One year after the vector delivery the animals were processed for immunohistochemical labeling of tyrosine hydroxylase (TH) to visualize dopaminergic SN neurons. Every sixth 50- μm -thick coronal section was used for counting. Pilot counts in control vector rats established that dissectors $50 \times 50 \mu\text{m}$ XY and $15 \mu\text{m}$ Z , spaced $100 \mu\text{m}$ apart, would suffice to generate counts in the range of

150–200 objects per animal (average total number of objects counted: control, 190 ± 17 , $N = 7$; α -syn, 157 ± 14 , $N = 8$). In principle the fractionator is insensitive to the size of dissectors provided that sampling is uniform and the probes are anisotropic ([15]; but cf. [18]). The average fractions of the total SN volume occupied by dissectors were 0.0332 ± 0.0027 of the total SN volume in animals that received control vector and 0.0241 ± 0.0005 in rats that received α -syn vector.

In sampling this 2–3% of the total volume of the SN there was no significant difference between control (0.59 ± 0.04 , $N = 7$) and α -syn (0.67 ± 0.10 , $N = 5$) brains in the average number of objects per dissector. Nor was there any difference in the distributions for the numbers of neurons found within dissectors (Figs. 4A and B). Thus it can be inferred from the count data that the gene transfer did not result in any significant change in the spatial density of SN TH neurons even though there was significant reduction in the estimated total number. This type of information leads to the testable hypothesis that the volume of the SN decreases as it loses its TH-immunoreactive neurons.

These data also illustrate how the error coefficient of the estimated number of neurons decreases asymptotically with increases in the number of objects counted (Fig. 4C). The limit to which the error decreases with increased number of objects counted is primarily a consequence of natural biological variation, decision errors in identification, and variability in section thickness measurements. For the eight animals injected with control vector, the section thickness coefficient of variation ($100\% \times \text{SE}/\text{mean}$) was 3.78%, which was more than half of the average c.e. If so, then the natural biological variation must account for less than half. The section thickness variability may arise from the mechanical imprecision of the frozen sectioning (true variation in section thickness), mechanical “slop” in the focus motor, and human errors in making the measurements. One recent report has described a potential introduction of bias related to shrinkage and other distortion associated with thick sections from nonembedded specimens [19].

With any localized treatment that affects how many objects actually exist in the samples, it is important to recognize that variation in factors such as injection placement can alter the error associated with number estimates and make it more difficult to determine to what extent various factors contribute to that error (Fig. 4D). Spatial gradients of cell death around a transfection locus for a toxic gene product will introduce heterogeneity in the spatial distribution of objects and increase the variation in the number of objects per dissector. However, even with a more variable relationship between the c.e. and the number of objects counted, seven of the eight α -syn vector animals had error coefficients <0.09 (range 0.0659–0.1005).

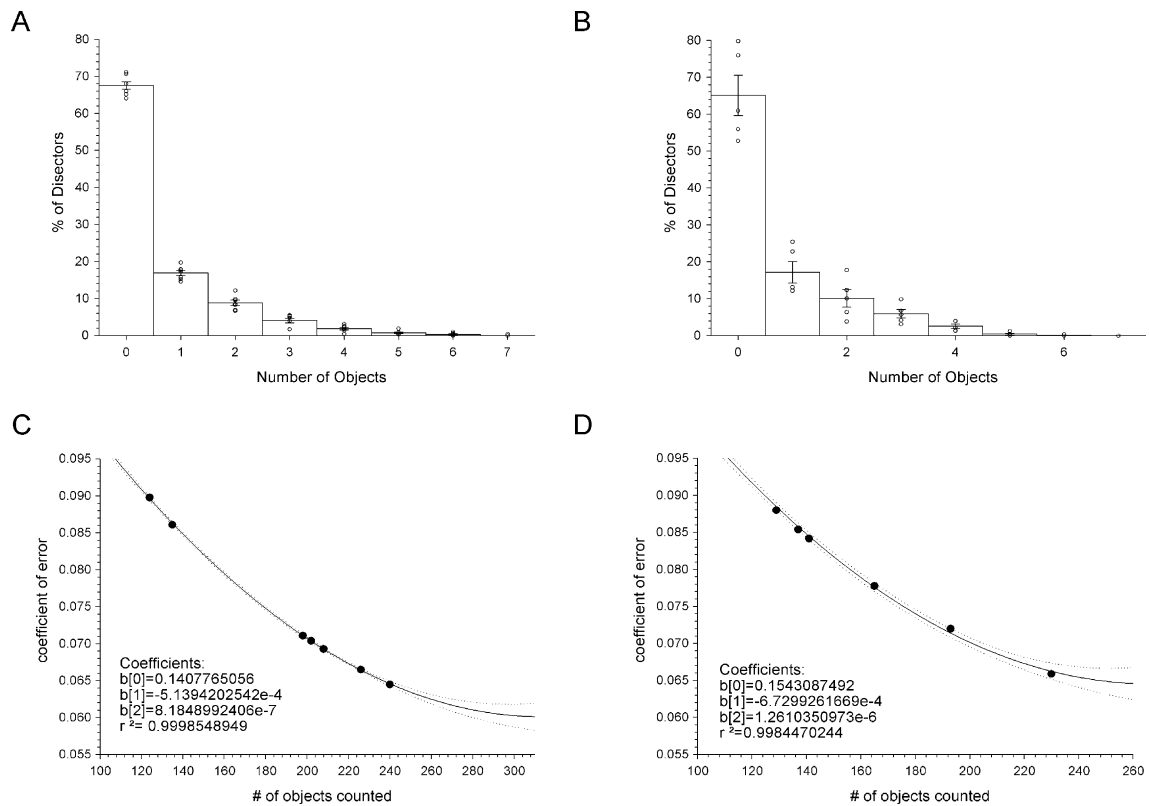


Fig. 4. (A) Number of objects counted per dissector, control vector. (B) Number of objects counted per dissector, α -syn vector. Counting diffusely localized immunolabeled neurons at magnifications high enough to permit shallow planes of focus results in more than half of all dissectors being empty. The similarity in the histograms suggests that the probability of locating a neuron within a randomly sampled volume (the spatial density) does not change in conjunction with the loss of immunolabeled neurons after α -syn gene transfer. (C) Coefficient of error for the estimated number of neurons decreases as the number of objects counted increases. A second degree polynomial fit illustrates the asymptotic relationship in control vector SN. Increasing the number of objects actually counted by increasing the number, size, or sampling frequency of dissectors will not reduce the precision of estimates beyond approximately 6–7%. (D) The asymptotic nature of this relationship is similar in the animals that received α -syn vector, even though a significant decrease in the average number of neurons was observed in the SN of the α -syn animals.

Using 40- μ m cresyl violet-stained frozen sections to count neurons in neocortex, the average time to complete each 15- μ m-deep optical dissector is about 30 s. In our α -syn gene transfer study we used between 118 and 397 dissectors per animal. With the dissector parameters optimized to count 150–200 cells, this means that the counting usually takes 1–3 h per animal. Changing the dimensions of the dissector does not substantially alter the time required for data collection. A faster computer, or increasing the Z stepping speed, might speed up the operation slightly but the rate-limiting step is the amount of time necessary for the user to traverse the dissector without making counting errors. This appears to be nearly optimal at the present rate, but can be adjusted somewhat for the preferences of the operator.

Manual object counting is typically quite simple when using high magnifications. For example, using a 100 \times oil immersion objective our standard 25 \times 25- μ m counting frame is approximately 6 by 8 cm on the 17-inch computer monitor, and magnified neuronal nucleoli can be as large as 1 cm across. Working with such enlargement results in much less operator fatigue than

counting through the eyepieces or on images projected through a drawing tube. Large objects, and those which are sparsely distributed in tissue samples, require larger count frames to limit the number without objects and hence lower counting magnifications. We customarily use 40–60 \times for counting immunolabeled neurons present at low densities in adult brains. This provides enough focal depth resolution to apply the counting rules, while keeping the number of zero-count dissectors to a minimum using count frames that fit within the microscope field of view.

As much as possible, we have constructed the macro to permit use of ImagePro Plus features outside the macros, and even other software applications apart from ImagePro Plus, during the execution of the fractionator process. Among other benefits, this makes the fractionator procedure compatible with the collection of additional stereological, morphometric, or densitometric data. For example, conventional point counting [11] could easily be done while the specimen is located at the dissector starting depth or measurements could be made of the integrated optical density or size

and shape characteristics (roundness, number of branches, etc.) of selected structures. The systematic random sampling could even be layered to sample different objects at different scales. For example, confocal resolution of mitochondria would permit fractionator number-per-cell estimates within cells that satisfied unbiased cell counting criteria. Improvements in computer power will also make it increasingly practical to generate truly isotropic (randomly sampled with respect to tissue orientation) disectors (cf. [21,22]).

Combined with the costs for a reasonably powerful desktop computer, a quality frame grabber, a good video graphics monitor, a video camera, and the ImagePro Plus package, the system that we have assembled is fairly expensive, not including a microscope. Although these costs still probably prohibit many microscopists from adopting stereological techniques, our system compares favorably with the available turnkey stereological systems on the market because it is capable not only of stereological analyses but also of integrated general digital imaging applications such as densitometry, image processing, and conventional histomorphometry. In addition, the costs for many of the individual component items are decreasing as new products come to market, and less expensive components than those used in our system are presently available. The ImagePro Plus software supports frame grabbers, and stage/focus hardware, from a variety of vendors and is available for both Windows and Macintosh operating systems. There are also other stereological software collections available for the Macintosh (NIH Image, Stereology Macros) or PC [23], although they do not provide control of hardware for stage movement and focus control. Thus, microscopists will find a wide range of price and performance options in upgrading their present platforms to stereological capability.

The fractionator macros should be directly transportable to, or at least easily modifiable for, use on systems with components different from ours. In fact, although the command code may require substantive modification, the logic of the fractionator macros should translate for use with software packages other than ImagePro Plus.

The macros are made of a series of subroutines, which can easily be modified as desired. For instance, if archival images are not desired, the call to that subroutine can easily be commented out. Similarly, if the user does not anticipate performing three-dimensional reconstruction using the count region outlines, the code section involved in saving these to disk can be bypassed.

There remains considerable room for improvement in both the hardware and the software components of our system. The stage and focus motor controls on the Prior hardware are occasionally sluggish due to apparent quirks in serial port communication and suspend program action while certain commands finish executing.

As with most if not all application software packages, the user will find the occasional bug, irrational feature, and error in the current version of ImagePro Plus. For example, the StagePro module for acquiring tiled images fails unless more than one field is included; this is not always necessary and requires an inelegant work-around. Despite such minor flaws, we have not found any software or hardware problems that impede our fractionator applications to any substantial extent. Finally, not being professional programmers, we have probably not always employed the most efficient programming solutions in our script code. The system that we describe here should be considered a work in continual progress, with revisions and improvements incorporated as we encounter new experimental demands.

The macros for the optical fractionator are available by request from the corresponding author. A demonstration of computer screen shots through the procedure can be accessed online at <http://www.mbi.ufl.edu/Dept/King/fractionator/index.html>.

Acknowledgments

We acknowledge the Media Cybernetics Technical Support personnel and the ImagePro Internet Users Group for assistance with problems encountered in learning to use ImagePro Plus and developing the macros. Some programming solutions incorporated into the macros have been borrowed from code made publicly available through these groups. M.K. was supported by Veterans Administration Medical Research Project 0002 and NIA P01 AG10485. E.M., N.S., and R.K. were supported by NIA AG 10485. Funding for the stage and focus equipment was made possible by a grant from the University of Florida Office for Research, Technology, and Graduate Education (ORTGE).

References

- [1] K.S. Bankiewicz, J.L. Eberling, M. Kohutnicka, W. Jagust, P. Pivrotto, J. Bringas, J. Cunningham, T.F. Budinger, J. Harvey-White, *Exp. Neurol.* 164 (2000) 2–14.
- [2] R. Xu, C.G. Janson, M. Mastakov, P. Lawlor, D. Young, A. Mouralev, H. Fitzsimmons, K.-L. Choi, H. Ma, P. Leone, Q. Chen, B. Dicker, M.J. During, *Gene Ther.* 8 (2001) 1323–1332.
- [3] R.L. Klein, M.E. Hamby, A.C. Hirko, Y. Gong, S. Wang, J.A. Hughes, M.A. King, E.M. Meyer, *Exp. Neurol.* 176 (2002) 66–74.
- [4] G. Andsberg, Z. Kokaia, R.L. Klein, N. Muzyczka, O. Lindvall, R.J. Mandel, *Neurobiol. Disease* 9 (2002) 187–204.
- [5] D. Kirik, C. Rosenblad, C. Burger, C. Lundberg, T.E. Johansen, N. Muzyczka, R.J. Mandel, A. Bjorklund, *J. Neurosci.* 22 (2002) 2780–2791.
- [6] R.L. Klein, M.A. King, M.E. Hamby, E.M. Meyer, *Hum. Gene Ther.* 13 (2002) 605–612.
- [7] R.P. Bolender, *Microsc. Res. Technique* 21 (1992) 338–346.
- [8] R.E. Coggeshall, H.A. Lekan, *J. Comp. Neurol.* 364 (1996) 6–15.
- [9] T.M. Mayhew, *J. Neurocytol.* 21 (1992) 313–328.

- [10] B. Pakkenberg, H.J. Gundersen, *J. Neurol. Sci.* 129 (Suppl.) (1995) 65–67.
- [11] J.P. Royet, *Prog. Neurobiol.* 37 (1991) 433–474.
- [12] M.J. West, L. Slomianka, H.J. Gundersen, *Anat. Rec.* 231 (1991) 482–497.
- [13] C. Schmitz, P.R. Hof, *J. Chem. Neuroanat.* 20 (2000) 93–114.
- [14] H.J. Gundersen, *J. Microsc.* 143 (1986) 3–45.
- [15] H.J. Gundersen, P. Bagger, T.F. Bendtsen, S.M. Evans, L. Korbo, N. Marcussen, A. Moller, K. Nielsen, J.R. Nyengaard, B. Pakkenberg, F.B. Sorensen, A. Vesterby, M.J. West, *Acta Pathol. Microbiol. Immunol. Scand.* 96 (1988) 857–881.
- [16] J.I. Keuker, G.K. Vollmann-Honsdorf, E. Fuchs, *Brain Res. Brain Res. Protoc.* 7 (2001) 211–221.
- [17] R.P. Bolender, J.S. Charleston, *Microsc. Res. Technique* 25 (1993) 314–324.
- [18] A.J. Harding, G.M. Halliday, K. Cullen, *J. Neurosci. Methods* 51 (1994) 83–89.
- [19] K.A. Dorph-Petersen, J.R. Nyengaard, H.J. Gundersen, *J. Microsc.* 204 (2001) 232–246.
- [20] E.M. Glaser, P.D. Wilson, *J. Microsc.* 192 (1998) 163–171.
- [21] P.R. Mouton, A.M. Gokhale, N.L. Ward, M.J. West, *J. Microsc.* 206 (2002) 54–64.
- [22] J.O. Larsen, H.J. Gundersen, J. Nielsen, *J. Microsc.* 191 (1998) 238–248.
- [23] N.D. Pentcheff, R.P. Bolender, *Microsc. Res. Technique* 21 (1992) 347–354.